Materials Advances

ROYAL SOCIETY OF CHEMISTRY

PAPER

View Article Online
View Journal | View Issue

Check for updates

Cite this: *Mater. Adv.*, 2024, 5, 9673

Thermoresponsive scaffolds fabricated using covalent organic frameworks for the selective removal of water contaminants†

Safoora Gazvineh,[a] Siamak Beyranvand,[a] Sara Saki,[a] Mohammad Nemati,[a] Kai Ludwig,[b] Patrick Amsalem,[c] Thorstenn Schultz,[d] Chong Cheng[e] and Mohsen Adeli *[a]

Received 5th August 2024,
Accepted 11th November 2024

DOI: 10.1039/d4ma00792a

rsc.li/materials-advances

Well-defined channels and inert and hydrolyzable structures of covalent organic frameworks make them excellent templates for the construction of polymeric scaffolds with a defined topology and properties. In this work, we report on the synthesis of thermoresponsive PNIPAM scaffolds templated by boronate ester COFs. Polymerization of *N*-isopropylacrylamide by azobisisobutyronitrile, encapsulated in COF channels, followed by the removal of the host framework resulted in PNIPAM scaffolds. The obtained scaffolds displayed different sizes and morphologies depending on whether polymerization was performed in the presence or absence of a crosslinking agent. In the presence of a crosslinking agent, porous PNIPAM scaffolds retained the size and the morphology of the COF, while without a crosslinking agent spindle-like microstructures were obtained. Constructed scaffolds were highly thermoresponsive and their morphology changed dramatically upon small temperature variations. This property was used for the controlled and selective removal of dye impurities from water. UV/visible absorption spectra showed that the obtained porous PNIPAM scaffold could effectively adsorb cationic and anionic dyes such as methylene blue (MB), rhodamine B (RhB), and fluorescein (FL) from wastewater. FL and RhB were effectively adsorbed by this scaffold, but a lower affinity was observed for MB. The absorption capacity of the PNIPAM1 sponge for FL, RhB and MB was 231 mg g^{-1}, 245 mg g^{-1} and 36 mg g^{-1}, respectively. Taking advantage of the high adsorption capacity and recyclability of the absorbant, it can be used for wastewater treatment.

Open Access Article. Published on 11 November 2024. Downloaded on 1/10/2025 12:42:15 PM.
This article is licensed under a Creative Commons Attribution-NonCommercial 3.0 Unported Licence.

Introduction

2D and 3D polymeric scaffolds have emerged as a new class of functional materials with unique physicochemical, optical, electrical and mechanical properties.[1–4] They play pivotal roles in both scientific and industrial areas, including nanomedicine,[5] biocatalysis,[6] electronics,[7,8] photonics,[9] sensing,[10] and environmental technology.[11,12] Random crosslinking of polymer chains, however, results in undefined scaffolds in terms of junction points, pore size, topology and shape, which is manifested in their nonreproducible properties and behaviors.[13] Crosslinking of polymer chains using traditional polymerization but in a regular pattern is a competent and cost-effective methodology with high reproducibility through which polymer scaffolds with controlled topology and properties can be constructed.[14–16] Radical polymerization of vinyl polymers in coordination channels is an intriguing method for the fabrication of polymer scaffolds with defined structures.[17–19] The topology and geometry of the constructed scaffolds, to gain unique properties, can be tuned by the manipulation of the channel size and coordination sites.[13,20,21] Metal–organic frameworks (MOFs) are able to host monomers that match the size of their channels. The channel's geometry and metal coordination sites confine monomers in special conformations and force polymerization in regular forms that cannot be achieved by traditional polymerization.[22–24] The versatility of this method opens up new ways for the construction of new topologies of polymer networks with unusual geometries or fabrication of composites from immiscible polymers with interesting properties.[25,26] Based on the available empty spaces and their topography and reactive sites, 1D, 2D and 3D polymer

[a] *Faculty of Science, Department of Chemistry, Lorestan University, Khorramabad, Iran. E-mail: adeli.m@lu.ac.ir*
[b] *Forschungszentrum für Elektronenmikroskopie and Core Facility BioSupraMol, Institut für Chemie und Biochemie, Freie Universität Berlin, Fabeckstr. 36a, Berlin 14195, Germany*
[c] *Institut für Physik, Humboldt-Universität zu Berlin, Newtonstr. 15, Berlin 12489, Germany*
[d] *Helmholtz-Zentrum Berlin für Materialien und Energie GmbH, Berlin 14109, Germany*
[e] *College of Polymer Science and Engineering, State Key Laboratory of Polymer Materials Engineering, Sichuan University, Chengdu, 610065, China*

† Electronic supplementary information (ESI) available. See DOI: https://doi.org/10.1039/d4ma00792a

Open Access Article. Published on 11 November 2024. Downloaded on 1/10/2025 12:42:15 PM. This article is licensed under a Creative Commons Attribution-NonCommercial 3.0 Unported Licence.

structures with extraordinary properties can be fabricated using MOFs.[20,27–29] While MOFs are very efficient and useful templates for the construction of polymer scaffolds, they are not inert and ligand–metal interactions can influence the polymerization of monomers having heteroatoms.[30,31] For example, monomers bearing nitrogen atoms are able to coordinate with metal sites in MOFs, change their structures by ligand exchange[32,33] and deviate polymerization by fixing the monomers in a rigid configuration.[34] Covalent organic frameworks (COFs) with inert structures, in comparison with MOFs, defined channels and versatile functionality are excellent platforms[35–39] for different applications[40,41] ranging from electrochemistry to sensors.[42–45] The geometry of their monomers manifests in the size and topology of their channels,[46–48] providing empty spaces to host different molecules.[49–51] Boron-based COFs are 3D structures made of stacked layers and organized by the dynamic nature of their boronate ester bonds. Due to their integrity and crystallinity, they are well-defined hosts to confine guests in special configurations.

Water sources play an irreplaceable role in industry and life activities. However, large amounts of wastewater containing various pollutants, such as heavy metals, dyes, phenolic compounds, pesticides, *etc.* have been discharged into the environment.[52] Synthetic dyes are common types of pollutants that are continuously released into natural water causing serious adverse effects to the environment. Such dyes are widely used in different applications including textiles, tanning, cosmetics and food production. They are not biodegradable and cause drastic changes in the ecological conditions of aquatic animals and plants. This will adversely affect the aquatic environment, resulting in serious and significant damage including algal bloom, oxygen depletion, color, turbidity and bad odor as well as long-term risks such as the bioaccumulation of carcinogenic aromatic products and chlorine by-products in the environment.[53,54] Therefore, there is a high demand for developing new adsorbents to remove dyes from wastewater.[55,56]

In this work, we took advantage of these properties for the encapsulation of azobisisobutyronitrile (AIBN) and performed radical polymerization of *N*-isopropylacrylamide (NIPAM) inside the channels of COFs. Polymerization of NIPAM in the presence of a crosslinker followed by the removal of the template resulted in porous poly(*N*-isopropylacrylamide) (PNIPAM) scaffolds similar to the parent COF in terms of the shape and size. In the absence of a crosslinking agent, however, spindle-like PNIPAM scaffolds were obtained. The morphology of both types of scaffolds changed, dramatically, by crossing the lower critical solution temperature (LCST) of PNIPAM. Porous PNIPAM scaffolds were changed to compressed sheet-like structures by slight heating. This property was used for the controlled separation of water impurities.

Experimental section

Preparation of covalent organic frameworks (COFs)

1,4-Benzene diboronic acid (0.765 mmol, 0.1265 g) and 2,3,6,7,10,11-hexahydroxytriphenylene (0.310 mmol, 0.1005 g) were added to a mixture of acetonitrile (80 ml), dioxane (16 ml) and mesitylene (4 ml) without rotation and sonicated for 10 minutes. Then, the mixture was left in an oil bath under reflux (90 °C) for 18 hours. Next, the reaction was terminated and then the mixture was centrifuged and the supernatant was separated. The obtained precipitate was centrifuged 4 times in toluene and dried at 40 °C.

Synthesis of $PNIPAM_1$

The COF (0.1 g) was mixed with α,α′-azobisisobutyronitrile (1.82 mmol, 0.3 g) in acetonitrile (15 ml). The mixture was stirred at 50 °C for 24 h to incorporate an initiator into the COF channels. After 24 hours, in order to remove the initiators physically adsorbed on the surface of the COF, the solvent was evaporated and the product was dialyzed using a 14 kDa dialysis bag for 3 hours in acetone. Next, the product was dispersed in acetonitrile and *N*-isopropylacrylamide (2.11 mmol, 0.3 g) and *N*,*N*-methylenebisacrylamide (0.129 mmol, 0.2 g) were added to the dispersion. The reaction mixture was stirred for 30 minutes at room temperature under a nitrogen atmosphere and then stirred at 70 °C for 24 hours. Afterwards, the solvent was evaporated and the product was dialyzed with a 14 kDa dialysis bag in acetone for 3 hours. Then, the precipitate obtained was dried in a vacuum at room temperature.

Synthesis of PNIPAM2

The same reaction, as for the synthesis of PNIPAM1, was performed but without adding *N*,*N*-methylenebis(acrylamide).

Hydrolysis of the covalent organic framework and extraction of the polymer

In order to remove the covalent organic framework and extract the polymer, **1**⊃PNIPAM was incubated in an acidic solution with pH = 2–3 at room temperature for 10 days. Afterwards, the samples were sonicated for 30 min and then centrifuged. The supernatant containing COF segments and unreacted monomers was separated and the precipitate was collected. This process was repeated three times, and finally, the product was dialyzed using a MWCO 2 kDa dialysis bag in THF for 3 hours and distilled water for one day. The product was dried in a vacuum oven at 40 °C.

Preparation of the $PNIPAM_1$-sponge

A polyurethane sponge (1 cm^3) was incubated with a methanol solution (2 cc) of $PNIPAM_1$ (3 mg) for 20 minutes at room temperature. Then, the $PNIPAM_1$-sponge was dried at 80 °C for 90 minutes.

Dye removal

A solution of methylene blue, rhodamine B and fluorescein dyes was prepared at a concentration of 100 mg L^{-1}. Then, by diluting the initial solution for the test, standard solutions were prepared.

For each of the control dye solutions and the dye solution with the sample, a polyurethane sponge was cut into a volume of 1 cm^3 and placed in a 2 ml methanol solution containing 3 mg PNIPAM1, soaked in an oven and dried. Then, the sponges

© 2024 The Author(s). Published by the Royal Society of Chemistry

Open Access Article. Published on 11 November 2024. Downloaded on 1/10/2025 12:42:15 PM. This article is licensed under a Creative Commons Attribution-NonCommercial 3.0 Unported Licence.

containing 3 mg PNIPAM1 were gently placed in 5 ml of a dye solution of 20, 15, 10 and 5 ppm (rhodamine B, methylene blue and fluorescein) and these solutions were incubated for 24 hours without shaking under ambient conditions (25 °C). After 24 hours, it was observed that the adsorbent could absorb fluorescein and rhodamine B to a large extent and absorb methylene blue to a certain extent. To measure the dye absorption coefficient with a spectrophotometer, the absorbance value of all samples at λmax corresponding to each dye was obtained and compared with the standard curve. The dye absorption capacity q_t (mg g^{-1}) and the percentage of dye removal (%) R by the adsorbent at each time point were calculated. Our aim was to investigate the absorption of cationic and anionic dyes, which are some of the most important pollutants in water. The results showed that this polymer has the ability to absorb dyes that have a carbonyl group in their structure such as RhB and fluorescein better than the MB dye.

Results and discussion

PNIPAM scaffolds were synthesized by the radical polymerization of NIPAM inside the channels of a boron-based covalent organic framework (1) (Fig. 1a). AIBN was encapsulated in **1** by stirring their mixture in acetonitrile for 24 h. Purification of the product and removal of physically adsorbed AIBN followed by heating a solution of NIPAM monomers in the presence of a COF-encapsulated initiator led to a **1**⊃PNIPAM composite. Polymerization occurred inside the empty spaces of COFs where AIBN was encapsulated. Removing **1**, *via* hydrolysis in an acidic medium, resulted in PNIPAM scaffolds with different sizes and shapes, depending on whether polymerization was performed in the presence or absence of a crosslinker (Fig. 1a and Fig. S1, ESI†). The obtained $PNIPAM_1$ scaffolds retained the morphology of the COF template when polymerization was performed in the presence of *N*,*N*′-methylenebis(acrylamide) as the crosslinker (Fig. 1b–d and e–g). However, in the absence of this crosslinker, $PNIPAM_2$ scaffolds were not similar to their parent COF in terms of topology and the size (Fig. 1h–j). Production of the stable PNIPAM scaffolds in the presence and absence of the crosslinker indicated 3D polymerization of NIPAM monomers inside the channels and interlayers of the COF. In the absence of the crosslinker, however, 3D polymerization is probably accompanied by chain transfer reactions, leading to crosslinked and stable scaffolds.[57] PNIPAM scaffolds synthesized in the presence and absence of the crosslinker were abbreviated $PNIPAM_1$ and $PNIPAM_2$, respectively.

The stretching vibration absorption bands of the aromatic rings of **1**, at 1584 cm^{-1}/1348 cm^{-1}, and the carbonyl groups of PNIPAM at 1735 cm^{-1}, in the IR spectra of **1**⊃PNIPAM were assigned to the polymerization of NIPAM monomers inside the COF channels (Fig. 2a).

Disappearance of the absorption bands of **1**, after hydrolysis, indicates the preparation of template-free PNIPAM scaffolds. The weaker C–H absorption bands in the IR spectra of $PNIPAM_2$ at 2990 cm^{-1}, in comparison with those of $PNIPAM_1$, was due to the consumption of these bonds for the chain transfer reactions and covalent crosslinking. Homogenous growth of polymer chains inside COFs was manifested in the thermogravimetric analysis (TGA) of **1**⊃PNIPAM, because one main weight loss at 440–540 °C was observed for this compound. The lower thermal stability of PNIPAM scaffolds together with less weight loss below 440 °C, in comparison with **1**⊃PNIPAM, confirmed removing the COF platform by hydrolysis. The thermal stability of $PNIPAM_1$ was lower than that of $PNIPAM_2$ (∼38 °C), indicating a higher crosslinking degree for the latter (Fig. 2b). TGA analysis showed that $PNIPAM_1$ has a higher thermal stability than $PNIPAM_2$ because $PNIPAM_1$ was synthesized in the presence of a crosslinker and the structure of $PNIPAM_2$ was not supported by a crosslinker (Fig. 1 and 2b).

The peaks at 2θ 3.5°, 6°, 9°, and 26° in the powder X-ray diffraction patterns of **1**, which are indicated by an asterisk, belong to the (100), (110), (210) and (001) planes and indicate the crystalline structure of this compound (Fig. 2c).[35,58,59]

The XRD diffractogram of **1**⊃PNIPAM did not show signals of compound **1**. A reason for such observation could be the low COF content of this compound, which can be proved by the TGA data. However, the diffractogram of **1**⊃PNIPAM showed new sharp signals that can be assigned to the crystalline structure of this compound. The susceptibility of **1** to hydrolysis was investigated by the incubation of this compound in an acidic medium (0.05 M HCl) for 10 days. We needed to know how fast this template can be excluded from **1**⊃PNIPAM to obtain a template-free PNIPAM scaffold. The XRD diffractogram of the hydrolyzed **1** showed several new peaks in the range of 2θ 4°–10°, 12°–38° and 21.2°, 23°, and 38°, which were assigned to the disturbed structure and degradation of this compound (Fig. 2c). This was confirmed by the SEM images of **1** incubated in an aqueous acidic medium for different time frames, where a clear trend for the destruction of the COF with increasing incubation time was observed (Fig. S2, ESI†). Any sign for the crystalline structure of the COF was not observed in the diffractograms of neither **1**⊃PNIPAM composites nor $PNIPAM_1$ and $PNIPAM_2$, confirming the disruption of the crystalline structure of this compound by growing polymer networks and the removal of the host template by hydrolyzing in an acidic medium. Interestingly, PNIPAM scaffolds showed sharp peaks in their diffractograms, indicating crystalline structures of these materials. $PNIPAM_1$ and $PNIPAM_2$ showed similar peaks at 2θ 7.5° and 22° but the sharper peak of the latter corresponds to the more crystalline structure of this compound (Fig. 2c).[60,61]

The higher crystallinity of $PNIPAM_2$ can be related to the higher crosslinking density of this scaffold, which is in agreement with the IR and TGA results. Fig. 2d–f show the XPS survey spectra of **1**, **1**⊃PNIPAM and $PNIPAM_1$. These spectra reveal the presence of carbon and oxygen as the main components of all samples. Nitrogen is absent in compound **1** but present in **1**⊃PNIPAM and $PNIPAM_1$, demonstrating the successful incorporation of NIPAM into the COF as well as the persistence of PNIPAM after hydrolysis. Interestingly, boron was detected in **1** and **1**⊃PNIPAM, but did not exist in the XPS spectrum of $PNIPAM_1$, thereby proving the effective removal of the COF by

Open Access Article. Published on 11 November 2024. Downloaded on 1/10/2025 12:42:15 PM.
This article is licensed under a Creative Commons Attribution-NonCommercial 3.0 Unported Licence.

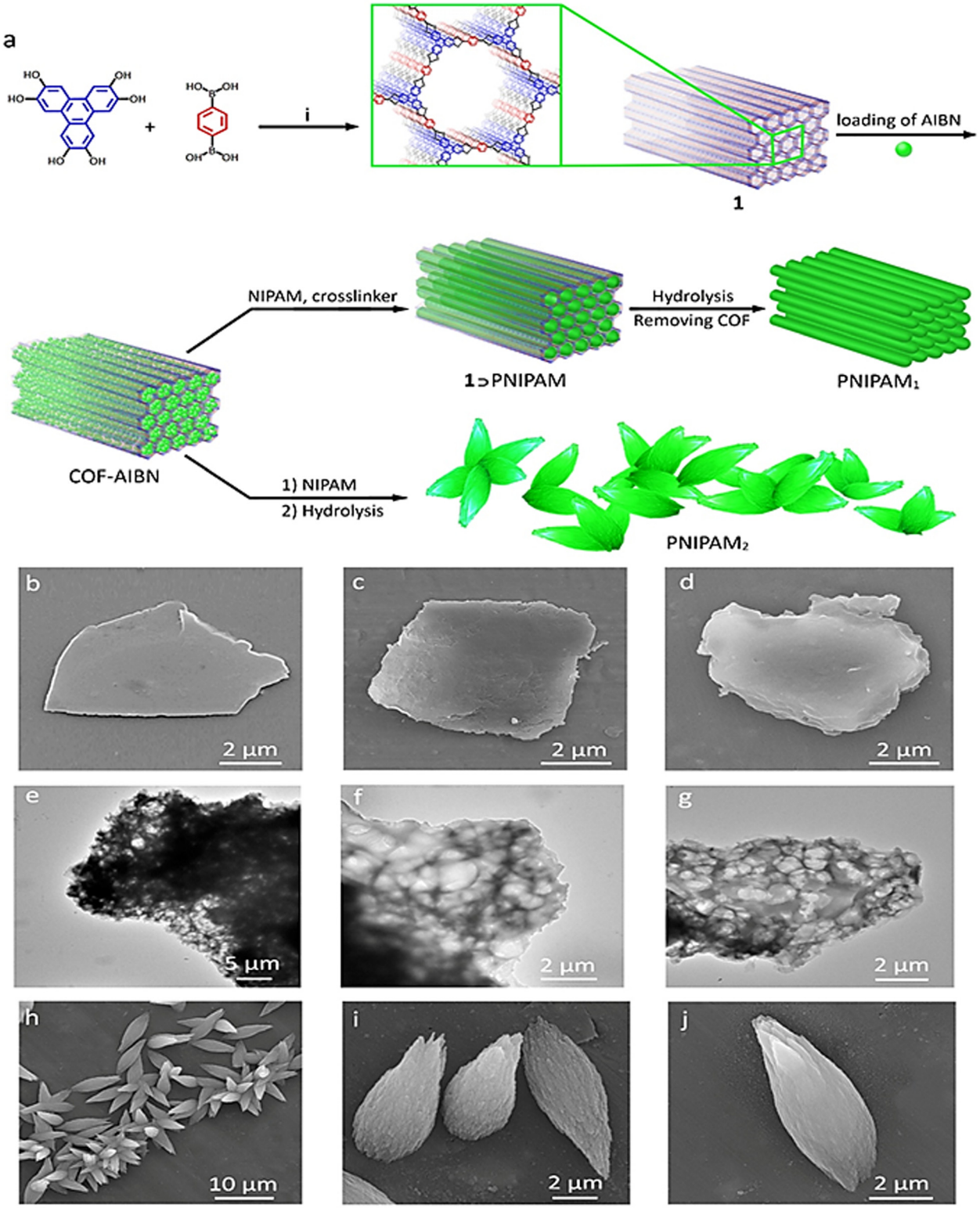

Fig. 1 (a) Schematic representation of the synthesis of PNIPAM scaffolds using boron-based covalent organic frameworks (i: acetonitrile, dioxane and mesitylene, 18 h, 90 °C). Encapsulation of AIBN inside COF channels followed by polymerization of NIPAM monomers in the presence and absence of the *N*,*N*′-methylenebis(acrylamide) crosslinker resulted in sheet-like and spindle-like PNIPAM scaffolds, respectively. SEM images of **1** (b), **1**⊃PNIPAM (c), $PNIPAM_1$ (d). (e)–(g) TEM images of the edges of $PNIPAM_1$. Scaffolds were too thick to be completely transmitted by the electron beam and pores were therefore only visible at the edges where the lower thickness allowed the fine structure to be observed. The size and shape of $PNIPAM_1$ was similar to that of the parent COF. SEM images of $PNIPAM_2$ (h)–(j). In the absence of the crosslinker spindle-like scaffolds were obtained.

© 2024 The Author(s). Published by the Royal Society of Chemistry

Open Access Article. Published on 11 November 2024. Downloaded on 1/10/2025 12:42:15 PM.
This article is licensed under a Creative Commons Attribution-NonCommercial 3.0 Unported Licence.

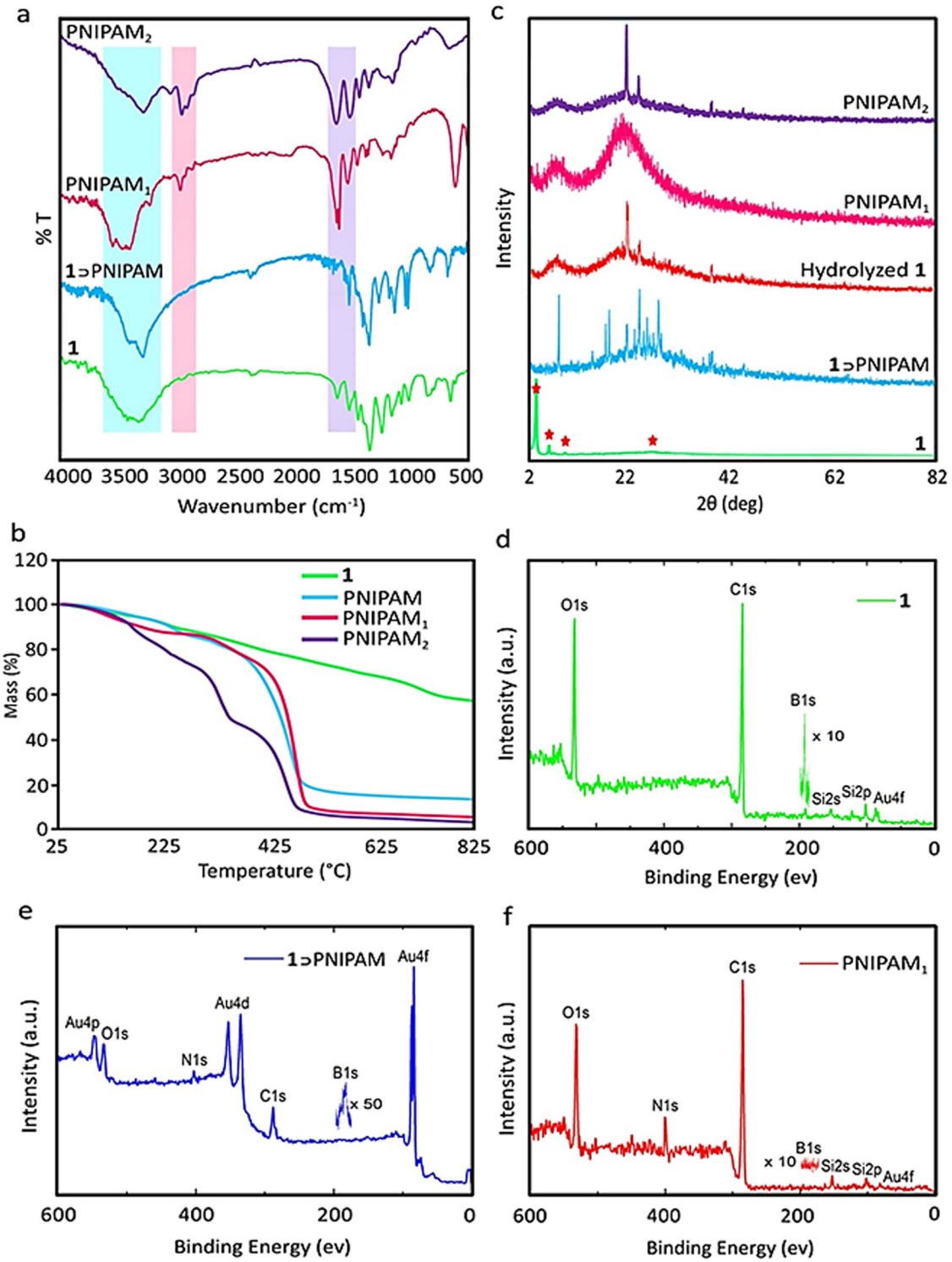

Fig. 2 (a) IR spectra of **1**, **1**⊃PNIPAM, $PNIPAM_1$ and $PNIPAM_2$. (b) XRD diffractograms of **1**, **1**⊃PNIPAM, hydrolyzed **1**, $PNIPAM_1$ and $PNIPAM_2$. (c) TGA thermograms of **1**, **1**⊃PNIPAM, $PNIPAM_1$ and $PNIPAM_2$. (d–f) XPS survey of **1**, **1**⊃PNIPAM and $PNIPAM_1$, respectively.

hydrolysis. Note that the observation of gold and silicon was related to the use of a gold-coated silicon substrate for the XPS measurements.

Thermoresponsive properties of the fabricated scaffolds were investigated. The clear solutions of PNIPAM scaffolds turned to turbid by heating up to 38 °C and the colloidal dispersions were precipitated at 39 °C after 10–15 minutes (Fig. 3a). After determining the LCST of PNIPAM scaffolds, more information regarding their thermoresponsive behavior was gained by electron microscopy. Solutions of the samples

Open Access Article. Published on 11 November 2024. Downloaded on 1/10/2025 12:42:15 PM.
This article is licensed under a Creative Commons Attribution-NonCommercial 3.0 Unported Licence.

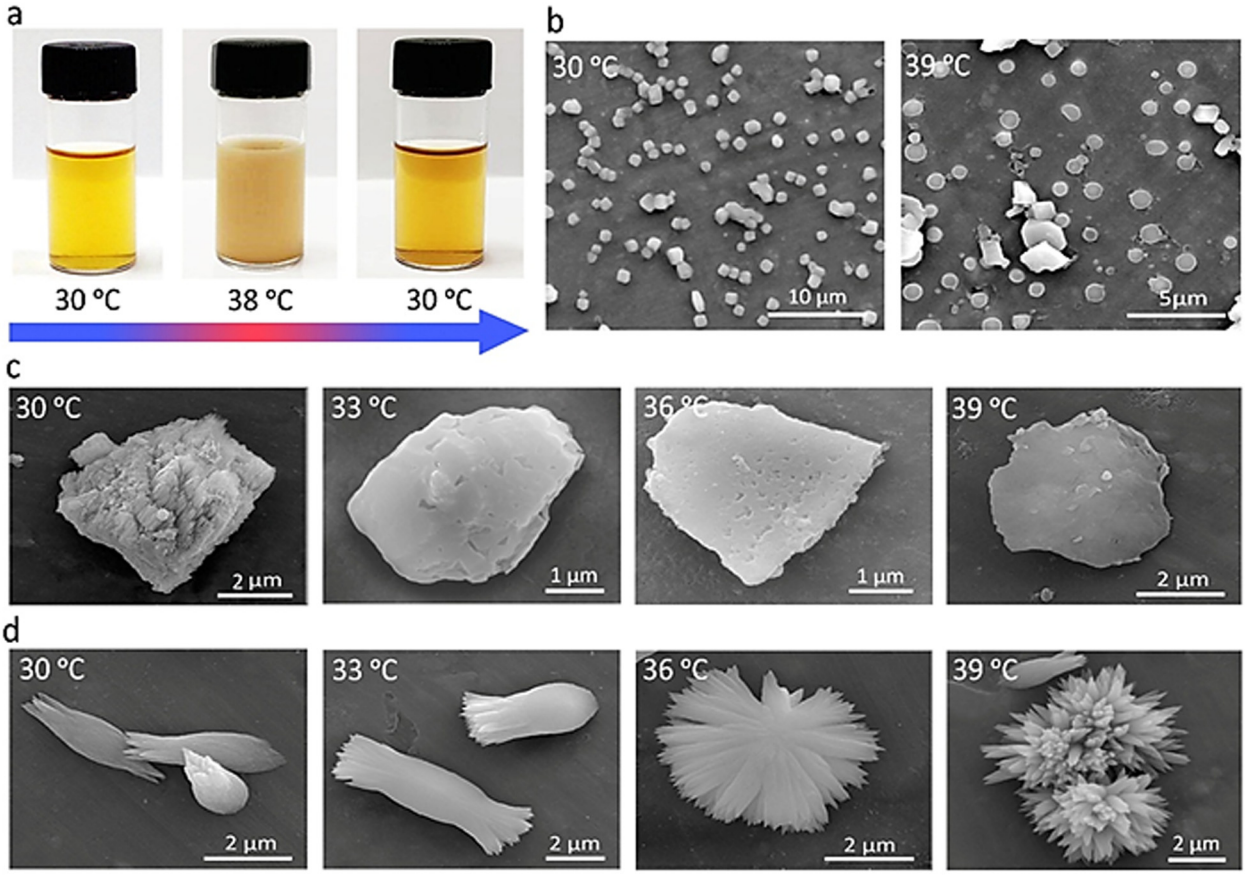

Fig. 3 (a) LCST of PNIPAM scaffolds was in the range of 36–38 °C. The colloidal dispersions were precipitated at 39 °C after 10–15 minutes. (b) SEM images of PNIPAM1 at 30 °C and 39 °C. SEM images of PNIPAM1 (c) and PNIPAM2 (d) at different temperatures ranging from 30 °C to 39 °C.

were dropped on the holder and dried at different temperatures and the SEM images were recorded. Clear differences were observed by looking at the structures of the scaffolds at temperatures lower and higher than their LCST. The crumpled 3D structures of $PNIPAM_1$ were changed to flat sheets by increasing the temperature to higher than their LCST (Fig. 3b and Fig. S4, ESI†).

The increased hydrophobicity of PNIPAM scaffolds at higher temperatures and pushing water molecules outside of the pores was manifested in a contracted structure. The SEM images of PNIPAM scaffolds were recorded with smaller temperature variations in the range of 30 °C to 39 °C. $PNIPAM_1$ gradually changed from a 3D scaffold toward sheet-like structures upon increasing temperature from 30 °C to 39 °C (Fig. 3c).

The morphology of $PNIPAM_2$ was even more thermosensitive and changed dramatically by slight changes in temperature. The heads of spindle-like $PNIPAM_2$ scaffolds were opened to create bouquet-like microstructures, increasing the temperature from 30 °C to 33 °C (Fig. 3d and Fig. S5, ESI†). Increasing the temperature to 36 °C and 39 °C changed the morphology of $PNIPAM_2$ from spindle-like microstructures to sunflower-like and globular structures, respectively (Fig. 3d and Fig. S5, ESI†). Persuaded by the thermo-switchable properties of $PNIPAM_1$, it was used for the selective removal of impurities from drinking water.

Methylene blue (MB), rhodamine B (RhB) and fluorescein (FL) are known water pollutants with adverse effects on the public health. The rate of their degradation is low and accumulate in nature upon discharging from different industries, posing a potential threat to humans. The accumulation of this cationic dye in the body may cause respiratory problems, rapid heartbeat, nausea, vomiting, abdominal pain, and skin irritation. Therefore, the removal of MB from relevant wastewater is essential. Moreover, they are charged dyes and investigation of their removal shed light on the role of electrostatic interactions at the dye/adsorbent interface. $PNIPAM_1$ (1 mg) was supported on polyurethane sponge (1 cm^3) for easy handling and separation of the adsorbed dye. $PNIPAM_1$-sponge was incubated with dye solutions (5 ml, 50 ppm) for 24 hours without shaking at 25 °C. FL and RhB were adsorbed by this scaffold efficiently but less affinity for MB was observed (Fig. 4).

The adsorption capacity of the $PNIPAM_1$-sponge for FL, RhB and MB was 231 mg g^{-1}, 245 mg g^{-1} and 36 mg g^{-1}, respectively (Table S2, ESI†). In comparison with similar systems, these obtained adsorption capacities are in a good level (Table 1).

Contaminated water samples were collected and the system performance was tested on them according to the test conditions described in the article for deionized water samples, and the results are reported in a table in the ESI† (Table S7).

© 2024 The Author(s). Published by the Royal Society of Chemistry

Open Access Article. Published on 11 November 2024. Downloaded on 1/10/2025 12:42:15 PM.
This article is licensed under a Creative Commons Attribution-NonCommercial 3.0 Unported Licence.

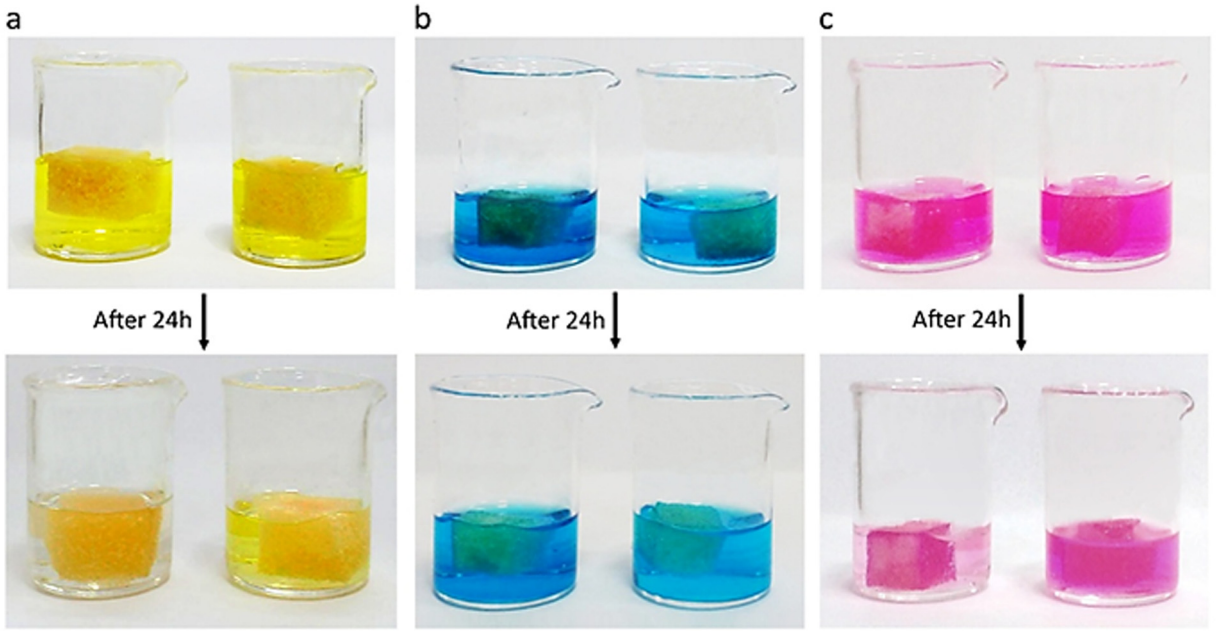

Fig. 4 Supporting $PNIPAM_1$ on a polyurethane sponge to remove dye impurities from water. Dye solutions (5 ml, 50 ppm) including (a) FL, (b) MB, and (c) RhB were incubated with the $PNIPAM_1$-sponge (left) and unmodified sponge (right) as the control for 24 h at room temperature and without shaking. FL and RhB solutions were almost colorless after 24 h incubation with the $PNIPAM_1$-sponge but the MB solution was still blue.

Table 1 Absorption capacity (mg g^{-1}) of the PNIPAM-sponge for dyes in comparison with similar systems

Adsorbent	Dye	Maximum adsorption capacity (mg g^{-1})	Ref.
PDVB-VI-*x*	RhB	260.42	62
γ-Fe_2O_3@Mt	RhB	209.20	63
MgAl-LDHs/sodium	RhB	59.64	
PANI/C	RhB	423.5	64
(MV)[BiI_3Cl_2]	FL	793	65
Silica microspheres (SM) with controlled hydrophobicity	FL	26–132	66
Tweezer-like adsorbent (CS–Ac–An)	FL	61.8	67
	FL	480.2	68
PNIPAM-sponge	RhB	245	This work
PNIPAM-sponge	FL	231	This work
PNIPAM-sponge	MB	98	This work

In order to understand the adsorption mechanism of dyes, the adsorption rate constants of the pseudo-first and second order kinetic models for each dye were investigated (Tables S3 and S4, ESI†).

Adsorption of dyes at different concentrations followed the pseudo-second-order kinetics. Fig. 5 shows the pseudo-first-order and pseudo-second-order kinetic models for the adsorption of RhB and FL onto sponge-loaded $PNIPAM_1$, having a better linearity fit for the second model. In addition, the calculated data of the kinetic model for the pseudo-second order were very close to the adsorption data, which indicated that the adsorption process in our work is consistent with the second-order kinetic model.

The Langmuir model was used for the prediction of the adsorption capacity of the $PNIPAM_1$-sponge, because its correlation coefficient (R^2) for the adsorption of FL, MB and RhB was larger than that of the Freundlich isotherm model (Fig. 6).

It can be concluded that dyes were adsorbed by the $PNIPAM_1$-sponge by noncovalent interactions and physical absorption, including hydrogen and electrostatic forces. Fitting parameters for both isotherms are summarized in Table S3 (ESI†).

Based on the Langmuir model, the dye molecules were adsorbed into the pores of the $PNIPAM_1$-sponge homogenously.[69–72] The homogenous adsorption of dyes indicated a homogenous structure for this scaffold. The calculated adsorption capacities using the Langmuir equation for FL, MB and RhB are shown in Table S5 (ESI†).

The thermodynamic parameters provide more information regarding the dye adsorption mechanisms (Fig. 7 and Table S6, ESI†).[73]

Adsorption of FL and RhB was exothermic with negative entropy but endothermic and positive entropy for MB (Fig. 8 and Table S6, ESI†). Interactions between dyes and $PNIPAM_1$ are exothermic because of electrostatic interactions and hydrogen bonding. Positive entropy for MB can be due to the dispersion of aggregations of this dye after interactions with the $PNIPAM_1$-sponge.

Open Access Article. Published on 11 November 2024. Downloaded on 1/10/2025 12:42:15 PM.
This article is licensed under a Creative Commons Attribution-NonCommercial 3.0 Unported Licence.

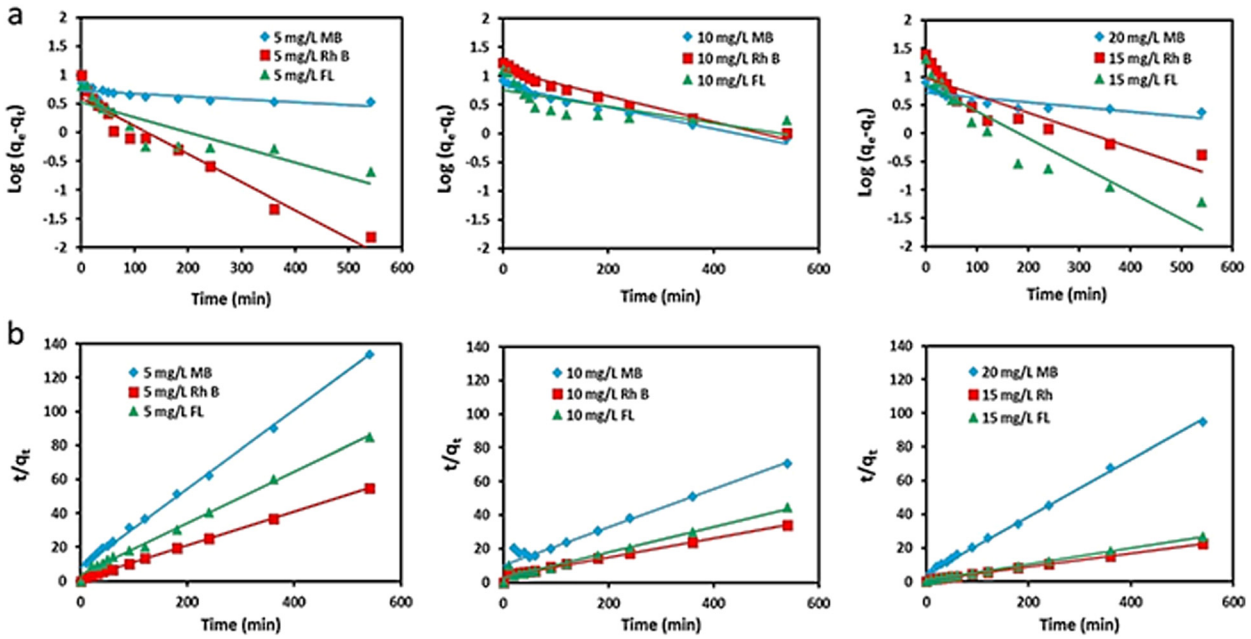

Fig. 5 The adsorption mechanism models of MB, RhB and FL by the PNIPAM1-sponge. (a) Pseudo-first-order kinetics model and (b) pseudo-second-order kinetics model.

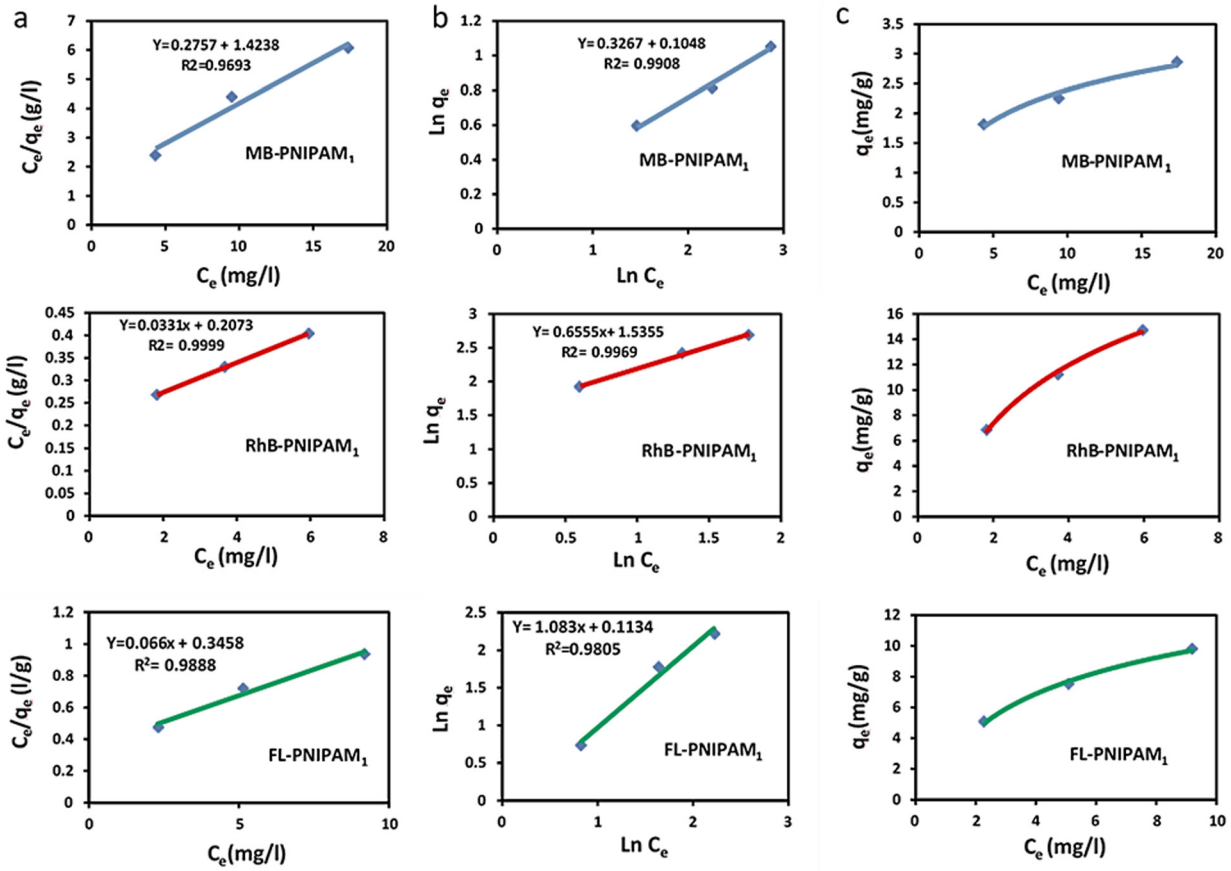

Fig. 6 (a) Langmuir isotherm models for the adsorption of MB, RhB and FL on the PNIPAM1-sponge. (b) Freundlich isotherm models for the adsorption of MB, RhB and FL on the PNIPAM1-sponge. (c) Adsorption isotherms of MB, RhB and FL on the PNIPAM1-sponge.

© 2024 The Author(s). Published by the Royal Society of Chemistry

Open Access Article. Published on 11 November 2024. Downloaded on 1/10/2025 12:42:15 PM.
This article is licensed under a Creative Commons Attribution-NonCommercial 3.0 Unported Licence.

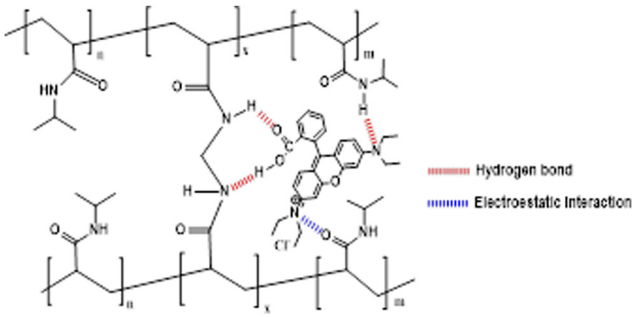

Fig. 7 Proposed mechanism for dye absorption, exemplified by Rhodamine B.

The efficient adsorption of FL and RhB and the accumulation of these dyes on/in the PNIPAM$_1$-sponge, however, result in negative entropy.

The thermosensitivity of the PNIPAM$_1$-sponge and the ability of this scaffold to release the captured dyes were investigated. The PNIPAM$_1$-sponge was incubated with aqueous solutions of dyes at 25 °C for one day and then the temperature was increased to 40 °C. Removal efficiencies and adsorption capacities were determined using UV-vis spectroscopy (Fig. 8a and b and Table S5, ESI†).

An inverse correlation between the R% and q_t (removal efficiency and adsorption capacity, respectively) *versus* temperature was observed for FL and RhB, due to exothermic interactions with the PNIPAM$_1$-sponge.

However, these parameters for MB were improved with increasing temperature, because positive entropy compensates the exothermic adsorption of the dye. The adsorption of FL and RhB decreased by raising the temperature but their desorption increased. MB showed an opposite behavior. As the temperature increased, the adsorption capacity of MB increased (Fig. 8b and Tables S5, S6, ESI†).

The ability of the PNIPAM$_1$-sponge for the controlled adsorption and release of dyes upon variation of the temperature was investigated. FL was adsorbed at 25 °C and then released by increasing the temperature to 40 °C. This is due to the lower affinity of the PNIPAM$_1$-sponge for this dye at higher temperatures. This thermosensitivity provides a strategy to remove dye impurities from water and concentrate them in a reservoir (Fig. 8a).

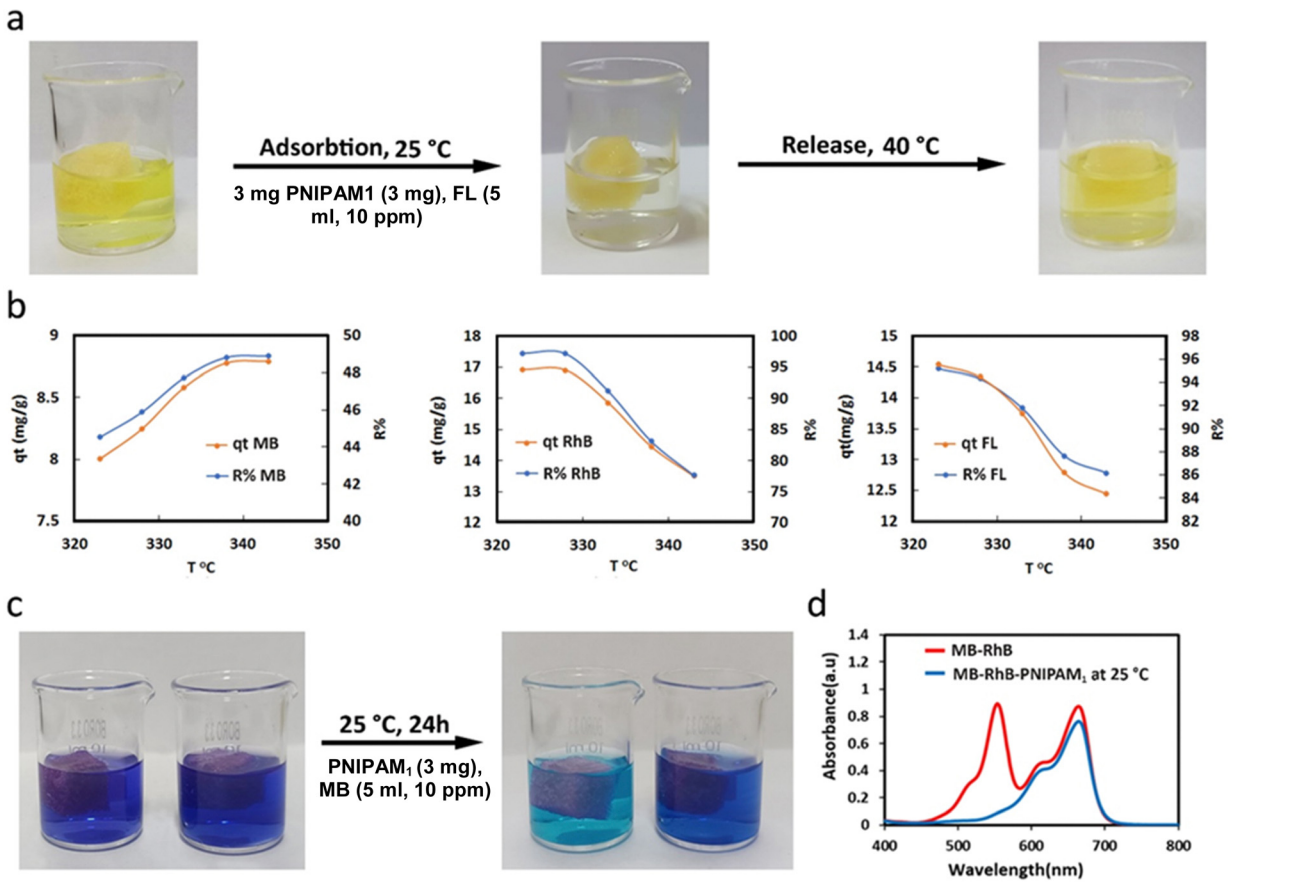

Fig. 8 (a) Efficient adsorption of FL (10 ppm in 5 ml) by the PNIPAM$_1$-sponge at 25 °C and then release of the dye at 40 °C. (b) Profiles of the dye removal percentage (R%) and adsorption capacity (q_t) for MB, RhB and FL by the PNIPAM$_1$-sponge *versus* temperature. Water solution of dyes (10 mg L^{-1}) was incubated with the PNIPAM$_1$-sponge at different temperatures and then removal of the dyes was determined by UV spectra. (c) and (d) Mixture of MB and RhB (10 ppm) was incubated with the PNAMAM$_1$-sponge and dye removal was visually or by UV-vis evaluated. A purple solution of RhB (red) and MB (blue) was changed to light blue, indicating intensive removal of RhB. The UV-vis spectra of RhB and MB (10 ppm) before and after incubation with the PNIPAM$_1$-sponge.

Open Access Article. Published on 11 November 2024. Downloaded on 1/10/2025 12:42:15 PM. This article is licensed under a Creative Commons Attribution-NonCommercial 3.0 Unported Licence.

The affinity of the $PNIPAM_1$-sponge to remove one dye from a mixture was also evaluated by incubation with a mixture of MB and RhB (10 ppm) at 25 °C. The UV spectra showed that RhB was completely removed by the $PNIPAM_1$-sponge, but MB was partially adsorbed (Fig. 8c and d). Therefore, it can be concluded that the $PNIPAM_1$-sponge adsorbs RhB specifically to some extent.

The ability of the $PNIPAM_1$-sponge to remove dyes from tap water was investigated (Table S7, ESI†). Adsorption capacities were less than those in distilled water but still in a good range to be considered as an efficient adsorbent for contaminated tap water.

Conclusions

Thermoresponsive porous PNIPAM scaffolds were synthesized using covalent organic frameworks, as templates, and used for the selective adsorption of dye impurities from water. Depending on performing polymerization in the presence or absence of a crosslinker, the shape and morphology of PNIPAM scaffolds were different. The synthesized scaffolds showed thermoresponsive properties at a LCST of 38 °C and were able to load and separate different dyes from water selectively. The precise morphologies, versatility and inertness of channels as well as the hydrolysable structure of COFs open up new avenues to construct polymeric networks with defined shapes and porosities that can be used for a wide range of future applications.

Data availability

The data and necessary protocols of this study have been included as part of the ESI.†

Conflicts of interest

There are no conflicts to declare.

Acknowledgements

We would like to thank the Iran Science Elites Federation and the Iran National Science Foundation (Project Number 4001281) for the financial support.

Notes and references

1 P. Kumbhakar, J. S. Jayan, A. S. Madhavikutty, P. Sreeram, S. Appukuttan, T. Ito and C. S. Tiwary, *iScience*, 2023, **26**(5), 106671.
2 A. M. Evans, M. J. Strauss, A. R. Corcos, Z. Hirani, W. Ji, L. S. Hamachi, X. Aguilar-Enriquez, A. D. Chavez, B. J. Smith and W. R. Dichtel, *Chem. Rev.*, 2021, **122**, 442–564.
3 Y. Liu, J. Huang, F. Zhou, L. Ni, Y. Shen, W. Liu and F. Meng, *Nanotechnol. Rev.*, 2021, **10**, 1425–1437.
4 Y. Noda, C. Merschjann, J. Tarábek, P. Amsalem, N. Koch and M. J. Bojdys, *Angew. Chem., Int. Ed.*, 2019, **58**, 9394–9398.
5 M. J. Mitchell, M. M. Billingsley, R. M. Haley, M. E. Wechsler, N. A. Peppas and R. Langer, *Nat. Rev. Drug Discovery*, 2021, **20**, 101–124.
6 A. Rodriguez-Abetxuko, D. Sánchez-deAlcázar, P. Muñumer and A. Beloqui, *Front. Bioeng. Biotechnol.*, 2020, **8**, 830.
7 H. Yuk, B. Lu, S. Lin, K. Qu, J. Xu, J. Luo and X. Zhao, *Nat. Commun.*, 2020, **11**, 1–8.
8 M. Oschatz, M. Zeiger, N. Jäckel, P. Strubel, L. Borchardt, R. Reinhold, W. Nickel, J. Eckert, V. Presser and S. Kaskel, *J. Mater. Chem. A*, 2015, **3**, 17983–17990.
9 A. F. Demirörs, E. Poloni, M. Chiesa, F. L. Bargardi, M. R. Binelli, W. Woigk, L. D. de Castro, N. Kleger, F. B. Coulter and A. Sicher, *Nat. Commun.*, 2022, **13**, 1–9.
10 J. Walker and M. Santoro, *Bioresorbable Polymers for Biomedical Applications*, Elsevier, 2017, pp. 181–203.
11 Z. Zhang, P. Bhauriyal, H. Sahabudeen, Z. Wang, X. Liu, M. Hambsch, S. C. Mannsfeld, R. Dong, T. Heine and X. Feng, *Nat. Commun.*, 2022, **13**, 1–9.
12 B. Le Ouay, H. Takaya and T. Uemura, *J. Am. Chem. Soc.*, 2019, **141**, 14549–14553.
13 S. Begum, Z. Hassan, S. Brase and M. Tsotsalas, *Langmuir*, 2020, **36**, 10657–10673.
14 J. Chen, E. S. Garcia and S. C. Zimmerman, *Acc. Chem. Res.*, 2020, **53**, 1244–1256.
15 S. Połowiński, *Prog. Polym. Sci.*, 2002, **27**, 537–577.
16 Y. Tang, D. Dubbeldam and S. Tanase, *ACS Appl. Mater. Interfaces*, 2019, **11**, 41383–41393.
17 T. Uemura, T. Kaseda and S. Kitagawa, *Chem. Mater.*, 2013, **25**, 3772–3776.
18 J. Ha, J. H. Lee and H. R. Moon, *Inorg. Chem. Front.*, 2020, **7**, 12–27.
19 B. Cai, S. Zhang and Y. Zhou, *CCS Chem.*, 2022, **4**, 1337–1346.
20 N. Hosono, S. Mochizuki, Y. Hayashi and T. Uemura, *Nat. Commun.*, 2020, **11**, 1–8.
21 K. Kokado, *Polym. J.*, 2017, **49**, 345–353.
22 T. Uemura, Y. Ono, Y. Hijikata and S. Kitagawa, *J. Am. Chem. Soc.*, 2010, **132**, 4917–4924.
23 D. Wang, Y. Xue, C. Wang, J. Ji, Z. Zhou and C. Tang, *J. Mater. Sci.*, 2019, **54**, 10168–10178.
24 L. Xie, K.-Y. Chan and N. Quirke, *Langmuir*, 2017, **33**, 11746–11753.
25 M. Rivera-Torrente, P. D. Pletcher, M. K. Jongkind, N. Nikolopoulos and B. M. Weckhuysen, *ACS Catal.*, 2019, **9**, 3059–3069.
26 N. Hosono and T. Uemura, *Matter*, 2020, **3**, 652–663.
27 L. Gao, C.-Y. V. Li, K.-Y. Chan and Z.-N. Chen, *J. Am. Chem. Soc.*, 2014, **136**, 7209–7212.
28 O. M. Planes, P. A. Schouwink, J. L. Bila, F. Fadaei-Tirani, R. Scopelliti and K. Severin, *Cryst. Growth Des.*, 2020, **20**, 1394–1399.
29 A. Acharjya, L. Longworth-Dunbar, J. r m Roeser, P. Pachfule and A. Thomas, *J. Am. Chem. Soc.*, 2020, **142**, 14033–14038.
30 T. Uemura, D. Hiramatsu, Y. Kubota, M. Takata and S. Kitagawa, *Angew. Chem., Int. Ed.*, 2007, **46**, 4987–4990.
31 T. Uemura, N. Uchida, M. Higuchi and S. Kitagawa, *Macromolecules*, 2011, **44**, 2693–2697.

© 2024 The Author(s). Published by the Royal Society of Chemistry

Open Access Article. Published on 11 November 2024. Downloaded on 1/10/2025 12:42:15 PM. This article is licensed under a Creative Commons Attribution-NonCommercial 3.0 Unported Licence.

32 D. Yu, Q. Shao, Q. Song, J. Cui, Y. Zhang, B. Wu, L. Ge, Y. Wang, Y. Zhang and Y. Qin, *Nat. Commun.*, 2020, **11**, 1–10.
33 Y. He, X. Lin, J. Chen, Z. Guo and H. Zhan, *ACS Appl. Mater. Interfaces*, 2020, **12**, 41942–41949.
34 Y.-S. Wei, M. Zhang, P.-Q. Liao, R.-B. Lin, T.-Y. Li, G. Shao, J.-P. Zhang and X.-M. Chen, *Nat. Commun.*, 2015, **6**, 1–7.
35 A. P. Cote, A. I. Benin, N. W. Ockwig, M. O'Keeffe, A. J. Matzger and O. M. Yaghi, *Science*, 2005, **310**, 1166–1170.
36 T. Ma, E. A. Kapustin, S. X. Yin, L. Liang, Z. Zhou, J. Niu, L.-H. Li, Y. Wang, J. Su and J. Li, *Science*, 2018, **361**, 48–52.
37 C. Zhao, H. Lyu, Z. Ji, C. Zhu and O. M. Yaghi, *J. Am. Chem. Soc.*, 2020, **142**, 14450–14454.
38 C. Feriante, A. M. Evans, S. Jhulki, I. Castano, M. J. Strauss, S. Barlow, W. R. Dichtel and S. R. Marder, *J. Am. Chem. Soc.*, 2020, **142**, 18637–18644.
39 C. R. DeBlase and W. R. Dichtel, *Macromolecules*, 2016, **49**, 5297–5305.
40 H. Lyu, H. Li, N. Hanikel, K. Wang and O. M. Yaghi, *J. Am. Chem. Soc.*, 2022, **144**, 12989–12995.
41 H. R. Abuzeid, A. F. EL-Mahdy and S.-W. Kuo, *Giant*, 2021, **6**, 100054.
42 X. Zhao, P. Pachfule and A. Thomas, *Chem. Soc. Rev.*, 2021, **50**, 6871–6913.
43 Y.-J. Li, W.-R. Cui, Q.-Q. Jiang, Q. Wu, R.-P. Liang, Q.-X. Luo and J.-D. Qiu, *Nat. Commun.*, 2021, **12**, 1–11.
44 G. Das, B. Garai, T. Prakasam, F. Benyettou, S. Varghese, S. K. Sharma, F. Gándara, R. Pasricha, M. Baias and R. Jagannathan, *Nat. Commun.*, 2022, **13**, 1–12.
45 M. Kou, W. Liu, Y. Wang, J. Huang, Y. Chen, Y. Zhou, Y. Chen, M. Ma, K. Lei and H. Xie, *Appl. Catal., B*, 2021, **291**, 120146.
46 K. Geng, T. He, R. Liu, S. Dalapati, K. T. Tan, Z. Li, S. Tao, Y. Gong, Q. Jiang and D. Jiang, *Chem. Rev.*, 2020, **120**, 8814–8933.
47 S. Dalapati, M. Addicoat, S. Jin, T. Sakurai, J. Gao, H. Xu, S. Irle, S. Seki and D. Jiang, *Nat. Commun.*, 2015, **6**, 1–8.
48 C. Gropp, T. Ma, N. Hanikel and O. M. Yaghi, *Science*, 2020, **370**, eabd6406.
49 J. L. Fenton, D. W. Burke, D. Qian, M. Olvera de la Cruz and W. R. Dichtel, *J. Am. Chem. Soc.*, 2021, **143**, 1466–1473.
50 B. Wang, X. Liu, P. Gong, X. Ge, Z. Liu and J. You, *Chem. Commun.*, 2020, **56**, 519–522.
51 Y. Zeng, R. Zou and Y. Zhao, *Adv. Mater.*, 2016, **28**, 2855–2873.
52 P. Bhatt, S. Gangola, G. Bhandari, W. Zhang, D. Maithani, S. Mishra and S. Chen, *Chemosphere*, 2021, **268**, 128827.
53 N. Stollberg, S. D. Kröger, M. Reininghaus, J. Forberger, G. Witt and M. Brenner, *Chemosphere*, 2021, **279**, 130480.
54 B. Hu, Q. Hu, C. Chen, Y. Sun, D. Xu and G. Sheng, *Chem. Eng. J.*, 2017, **322**, 66–72.
55 J. Li, X. Liu, G. Zhao, Z. Liu, Y. Cai, S. Wang, C. Shen, B. Hu and X. Wang, *Sci. Total Environ.*, 2023, **869**, 161767.
56 B. Wang, Y. Li, J. Zheng, Y. Hu, X. Wang and B. Hu, *Chemosphere*, 2020, **254**, 126898.
57 W. Wu, J. Liu, P. Gong, Z. Li, C. Ke, Y. Qian, H. Luo, L. Xiao, F. Zhou and W. Liu, *Small*, 2022, **18**, 2202510.
58 D. Hao, J. Zhang, H. Lu, W. Leng, R. Ge, X. Dai and Y. Gao, *Chem. Commun.*, 2014, **50**, 1462–1464.
59 S. Kim, C. Park, M. Lee, I. Song, J. Kim, M. Lee, J. Jung, Y. Kim, H. Lim and H. C. Choi, *Adv. Funct. Mater.*, 2017, **27**, 1700925.
60 Y. Wang, S. Song, X. Chu, W. Feng, J. Li, X. Huang, N. Zhou and J. Shen, *Colloids Surf., A*, 2021, **612**, 125987.
61 I.-C. Radu, I.-E. Biru, C.-M. Damian, A.-C. Ion, H. Iovu, E. Tanasa, C. Zaharia and B. Galateanu, *Molecules*, 2019, **24**, 4096.
62 Y. Han, W. Li, J. Zhang, H. Meng, Y. Xu and X. Zhang, *RSC Adv.*, 2015, **5**, 104915–104922.
63 H. Ouachtak, R. El Haouti, A. El Guerdaoui, R. Haounati, E. Amaterz, A. A. Addi, F. Akbal and M. L. Taha, *J. Mol. Liq.*, 2020, **309**, 113142.
64 M. Adel Sayed, A. Mohamed, S. A. Ahmed, A. M. El-Sherbeeny, W. Al Zoubi and M. R. Abukhadra, *ACS Omega*, 2023, **8**, 47210–47223.
65 J. Wang, J. Zheng, S. Wang, J. Sun, Y. Guo, H. Wang, S. Huang, Y. Li and C. Wang, *Mater. Lett.*, 2019, **254**, 419–422.
66 I. V. Melnyk, V. V. Tomina, N. V. Stolyarchuk, G. A. Seisenbaeva and V. G. Kessler, *J. Mol. Liq.*, 2021, **336**, 116301.
67 B. Vafakish and L. D. Wilson, *Surfaces*, 2019, **2**, 468–484.
68 S. Jia, S. Song and X. Zhao, *Appl. Organomet. Chem.*, 2021, **35**, e6314.
69 Y. Zhang, X. Hong, X.-M. Cao, X.-Q. Huang, B. Hu, S.-Y. Ding and H. Lin, *ACS Appl. Mater. Interfaces*, 2021, **13**, 6359–6366.
70 M. J. Pirouz, M. H. Amini and M. H. Beyki, *Desalin. Water Treat.*, 2021, **227**, 360–369.
71 L. Wang, Y. Tao, J. Wang, M. Tian, S. Liu, T. Quan, L. Yang, D. Wang, X. Li and D. Gao, *Anal. Chim. Acta*, 2022, **1227**, 340329.
72 S.-X. Xu, Z.-Q. Yao and Y.-H. Zhang, *Eur. Polym. J.*, 2020, **133**, 109764.
73 I. Ghosh, S. Kar, T. Chatterjee, N. Bar and S. K. Das, *Process Saf. Environ. Prot.*, 2021, **149**, 345–361.